Spectral study of the lateral trace-space of laser-driven proton beams

C. Salgado-López,[1,*] I. Rodríguez-Pérez,[1] J. I. Apiñaniz,[1] A. Curcio,[2] T. Cebriano,[1] A. Morabito,[1] L. Volpe,[1,3] and G. Gatti[1]

[1]Centro de Láseres Pulsados (CLPU), Edificio M5, Parque Científico USAL, C/ Adaja, 8, 37185 Villamayor, Salamanca, Spain
[2]SBAI Department, Sapienza University of Rome, Via Antonio Scarpa, 14, 00161 Rome, Italy
[3]ETSI Aeronáutica y del Espacio, Universidad Politécnica de Madrid, 28040 Madrid, Spain

(Received 8 May 2025; accepted 21 July 2025; published 23 September 2025)

The characterization of the phase space of laser-driven proton beams—particularly across a broad energy spectrum—in spite of the recent interest in laser-driven particle accelerators, remains a significant challenge due to the complex interplay between transverse dynamics and spectral properties. This work presents a detailed spectral study of the lateral emittance of laser-driven proton beams, providing energy-resolved, single-shot measurements of the beam emittance by means of a magnetically streaked pepper-pot method. Experimental results from a laser-driven proton source demonstrate the ability to resolve the beam's transverse trace space at various proton energies, yielding precise emittance estimations and highlighting the variation of beam quality with energy. The study emphasizes the necessity of high spectral resolution for accurate emittance characterization. The findings offer valuable implications for optimizing beamline design and improving the performance of future tabletop laser accelerators.

DOI: 10.1103/ltz6-gqk4

I. INTRODUCTION

Laser-driven particle accelerators have emerged as a promising approach for a variety of scientific and practical applications, partly due to their excellent transverse beam quality and ultrashort pulse duration [1–3]. Laser-driven ion beams have demonstrated their utility as diagnostics for fast plasma phenomena [4,5], warm dense matter generation [6], fusion energy studies [7,8], and several medical applications, comprising radioisotope production [9] and tumor irradiation [10], to name a few.

Most of these applications rely in the capacity of these ions to be manipulated, transported, and focalized by adequate beam magnetic optics [10,11]. Reduced focal volumes can be achieved due to the outstanding laminarity regime of the laser-generated proton beams through the target normal sheath acceleration (TNSA) process [1,2], resulting in a potential increase of the current and spatial resolution at the irradiation point.

Due to its major relevance in the transference toward possible applications, the evaluation of the laser-driven ion beam trace space is drawing increasing attention. The measurement of the complex relation between the space and divergence beam coordinates—and their dependency on the ion energy—in such beams has been addressed by very few methods in the past, such as the proton grid radiography [12–15] and target machining toward microfocusing fiducials [16–18], among others [19]. As shown in Fig. 1, these studies have yielded a dispersion of several orders of magnitude for the estimated values of transverse emittance (which is the figure of merit for the beam spatial quality), for rather similar interaction conditions [i.e., $\tau_L < 1\,\text{ps}$, $I\lambda^2 > 10^{18}\,\text{W}/(\text{cm}^2\,\mu\text{m}^2)$ and metallic foil target of thickness $L \sim 10\,\mu\text{m}$]. Moreover, emittance results seem to depend not only on the primary experimental parameters, but also on the measurement method, geometry of detection (distance from source and angular acceptance), and the spectral range selection [20]. In any case, these works showed remarkable low-emittance values for protons accelerated through the TNSA, considerably improving the quality of conventional ion accelerators. Such excellent transverse beam quality is attributed to the very transient nature of the accelerating field and the fact that such ions arise from an originally unperturbed plane surface. Emittance growth at the source is mainly attributed to the filamentation of the electron beam (responsible for the charge imbalance that accelerates the ions) close to the front surface of the target [21].

Most of the aforementioned trace-space retrieval methodologies rely on use of radiochromic films (RCFs) as particle detection, preventing a potential high-repetition-rate (HRR) evaluation of the beam parameters with sufficient energy resolution, far from the requirements of the operation rate of the high-power lasers systems (>1 Hz). In this work, a systematic study of the beam lateral trace space of a laser-driven proton beam is presented. A detailed energy-resolved, single-shot retrieval of the beam emittance is possible thanks to a different methodology based on a modified version of the pepper-pot technique.

*Contact author: csalgado@clpu.es

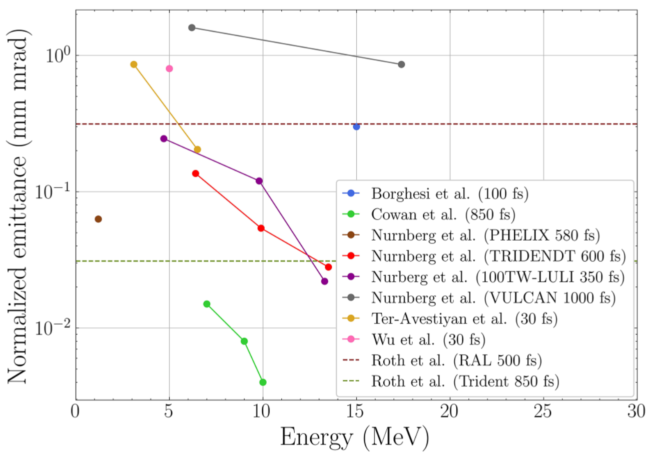

FIG. 1. Normalized emittance measurements of laser-driven proton beams at different energies found in the bibliography. Works without any energy specification are shown with dashed lines.

II. MAGNETICALLY STREAKED PEPPER-POT METHOD

Following Refs. [20,22–24], for a beam with a preferential direction z and transverse coordinate x (i.e., $p_z \gg px$ and $p_z \approx p$), a first definition of the one-dimensional beam emittance can be given from the transverse trace space (x, x'), where $x' = p_x/p$ is the divergence angle of the beam. The so-called root-mean-square (rms) trace-space emittance (or geometrical emittance) is defined as

$$\varepsilon_{\rm rms} = \sqrt{\langle x^2\rangle\langle x'^2\rangle - \langle xx'\rangle^2}, \qquad (1)$$

where $\langle\cdots\rangle$ corresponds to the statistical moments of the particle distribution. This quantity is proportional to the area occupied by the particles in the trace space, as well as to any nonlinearities in the relation between x and x', and it is conserved if no net acceleration is applied to the beam. A perfectly laminar particle stream shows $\varepsilon_{\rm rms} = 0$, corresponding to a beam originated from a pointlike virtual source whose particle trajectories never intersect.

On the other hand, emittance can also be determined in the beam phase space (x, p_x), named as normalized rms emittance:

$$\varepsilon_{n,\rm rms} = \frac{1}{mc}\sqrt{\langle x^2\rangle\langle p_x^2\rangle - \langle xp_x\rangle^2} = \sqrt{\langle x^2\rangle\langle\beta^2\gamma^2x'^2\rangle - \langle x\beta\gamma x'\rangle^2}, \qquad (2)$$

where $\beta = v/c$ and $\gamma = (1-\beta^2)^{-1/2}$. This quantity is not sensitive to longitudinal acceleration. Considering a nonrelativistic beam ($\gamma = 1$) and ignoring the coupling between energy and transverse position (as in a drift without collective effects), the normalized emittance can be expressed as

$$\varepsilon_{n,\rm rms}^2 = \langle\beta\rangle^2\left(\sigma_E^2\langle x^2\rangle\langle x'^2\rangle + \varepsilon_{\rm rms}\right), \qquad (3)$$

$\sigma_E^2 = \langle\beta^2\rangle - \langle\beta\rangle^2$ being the relative energy spread. This latter expression shows that both definitions of the emittance (in the phase space and the trace space) are equivalent for beam with insignificant energy spread. Nevertheless, this is not the case for laser-driven ion accelerators, which show extraordinarily large energy bandwidths. Equation (3) shows as well a rapid beam worsening behavior due to a combined effect of a large energy spread and a high beam divergence in a simple drift. All this evidences the importance of a trace-space characterization of the laser-driven beams with sufficient energy resolution as a mandatory step toward efficient beam manipulation and applications.

Pepper-pot is a well-known method for trace-space rms emittance measurement, which consists in the individual detection of *pieces* of the beam, which is physically split by a pinhole mask [23]. After some free flight distance L', the different beamlets are characterized by a spatially resolved detector, obtaining simultaneously information for space and divergence of each beamlet, allowing for a discretized measurement of the trace space. From that, it is possible to derive an expression for the geometrical rms emittance in one beam transverse dimension as [25]

$$\varepsilon_{\rm rms} \approx \frac{1}{N}\sqrt{\left\{\sum_i^p n_i(x_i - \langle x\rangle)^2\right\}\left\{\sum_i^p \left[n_i\sigma_i'^2 + n_i(\langle x_i'\rangle - \langle x'\rangle)^2\right]\right\} - \left\{\sum_i^p (n_i x_i\langle x_i'\rangle) - N\langle x\rangle\langle x'\rangle\right\}^2}, \qquad (4)$$

where p is the number of pinholes, n_i is the number of particles crossing the ith pinhole, N is the total number of particles detected, x_i is the ith pinhole position, $\langle x\rangle$ and $\langle x'\rangle$ are the main beam position and divergence, and $\langle x_i'\rangle$ and σ_i' are, respectively, the ith beamlet mean divergence and its rms width. This technique is designed for monoenergetic particle beams, but it can be addressed for broadband spectra by using energy-selective detectors, such as RCFs [19]. This technique has been reported as well for the emittance estimation of narrow spectral bands of laser-driven wakefield-accelerated electrons [26–29].

A modification of the conventional pepper-pot method has been conceived for detection of the large energy spread of the laser-driven proton beams. A one-dimensional pinhole mask discretizes the beam in one of its transverse axes; such beamlets are let to travel toward the detector, but they are deflected by a large magnetic field—sustained by a magnetic dipole—similarly as in a magnetic spectrometer, which deviates these beamlets in the orthogonal direction. The operation principle is summarized in Fig. 2. A modified version of a Thomson parabola (TP) spectrometer with angular resolution [30] was employed for such measurement. A 1.5-mm-thick BC-400 plastic scintillator was used as a proton trace detector, improving the angular acceptance of the device (due to its larger surface compared to a conventional microchannel plate) but still keeping the HRR operation and enough spatial resolution [31]. The front surface of the scintillator was shielded with a 12-μm-thick black-dyed polycarbonate opaque foil in

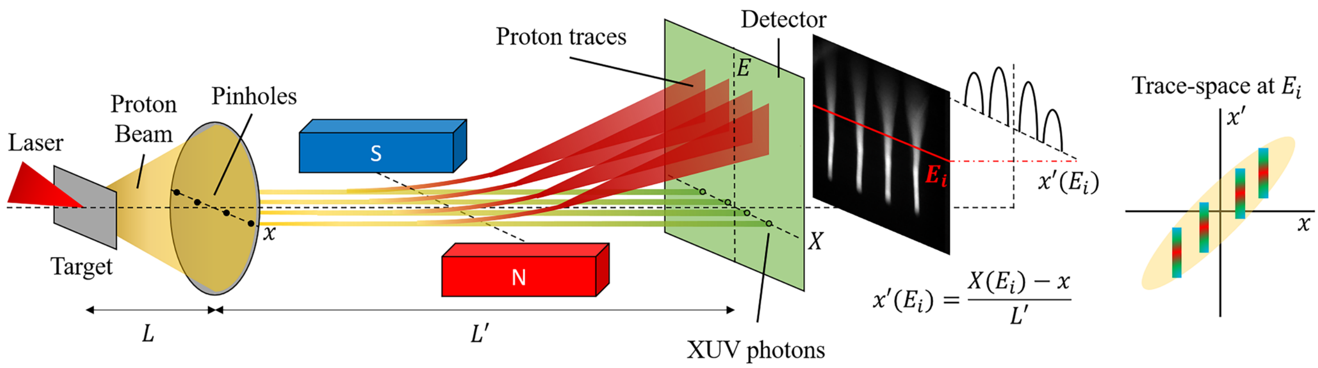

FIG. 2. Operation principle of the B-field streaked pepper-pot method for laser-driven proton beams. A mask of horizontally displayed pinholes (in this case, parallel to the laser beam polarization) is set at a distance L from the beam source. The selected beamlets travel a distance L' until a scintillating screen, while deflected vertically by a permanent magnetic dipole. The horizontal coordinate at the detector plane X_i encodes the information of the beam divergence x_i' at a beam coordinate x_i (i.e., the trace space), while the vertical coordinate spectrally resolves such data.

order to stop stray light and low-energy heavier ions. Protons were the only species of ions detected in such configuration (for the interaction conditions of the experiment), which was confirmed by ion separation when turning on the electric field of the TP. The absorption of the carbon ions in the plastic foil, as well the deposition of all the proton energy (up to 20 MeV) inside the bulk of the filter, was also checked by Monte Carlo code MCNP6 [32].

Following Ref. [23], certain conditions should be complied to allow for a proper estimation of the emittance. The proportionality relation between proton charge and the scintillating response should be applied to the detected signal of each trace [through n_i in Eq. (4)]. Taking into account that, in the case of a scintillator, such relation is purely dependent on the particle energy deposition and material thickness, the absolute calibration of the scintillating signal is not required when comparing traces at the same energy level. On the other hand, the spatial resolution should be sufficient to accurately estimate the trace centroids and rms widths. For such reasons, the distances from target to pinhole L and pinhole to detector L' were set such that $(L + L')/L \gg 1$, obtaining a large magnification factor for the pinhole imaging effect; the resulting millimeter-thick traces were easily resolved by a high-aperture imaging system onto a scientific camera.

III. EXPERIMENTAL DEMONSTRATION

A study of a TNSA-driven proton source was performed at the VEGA 3 pulsed laser system. Similar interaction conditions were achieved for every shot shown. The laser delivers 21.6 ± 0.9 J energy on target, with an FWHM duration of 247 ± 7 fs. These pulses are focused onto a 100-μm-thick Al foil by an $f/10$ off-axis parabolic mirror to a 14 ± 2 μm FWHM focal spot containing 29% of the total laser energy, resulting in an average intensity of $(1.6 \pm 0.4) \times 10^{19}$ W/cm^2 inside the FWHM. The angle of incidence of the laser axis is 12° with respect to the target normal. The laser is linearly polarized in the plane of incidence, and its central wavelength is 800 nm.

In order to optimize the pinhole magnification, the distance from the mask (with pinhole diameter 100 μm) to the proton source was set as $L = 15$ mm, so $(L + L')/L \gg 1$ for every shot. The scintillator longitudinal position could be changed between shots, resulting in two different trace magnifications with $L'/L = 15$ and $L'/L = 25$. In such geometrical configuration, only four traces could be detected due to the limited device angular acceptance—mainly constrained by dipole gap—spanning a beam divergence angle of 6°. The traces detected in a typical shot for $L'/L = 25$ are shown in Fig. 3.

The different terms of Eq. (4) can be estimated from the detected traces for different proton energies (i.e., for every magnetic deflection coordinate). It is worth mentioning that the rms trace divergence σ_i' was calculated after the deconvolution of the raw trace width with a point spread function (PSF), considered to be the square projection of the pinhole aperture onto the detector. σ_i' being the largest contribution to the emittance in this case, the resolution limit of this

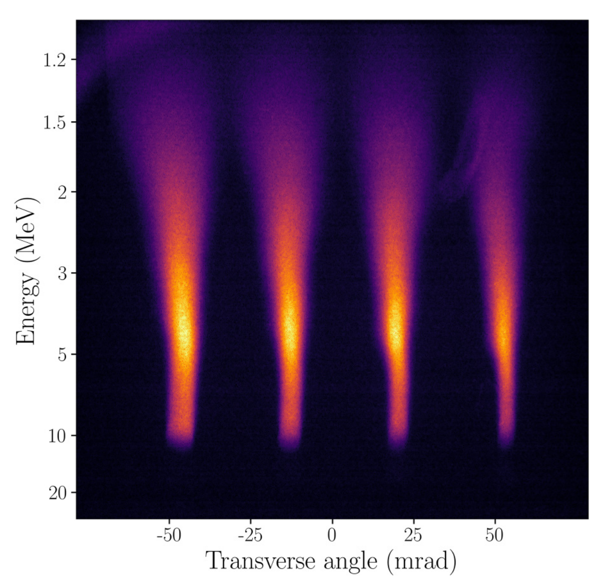

FIG. 3. False color image of the proton traces detected by the magnetically streaked pepper-pot method in a typical TNSA experiment at VEGA 3.

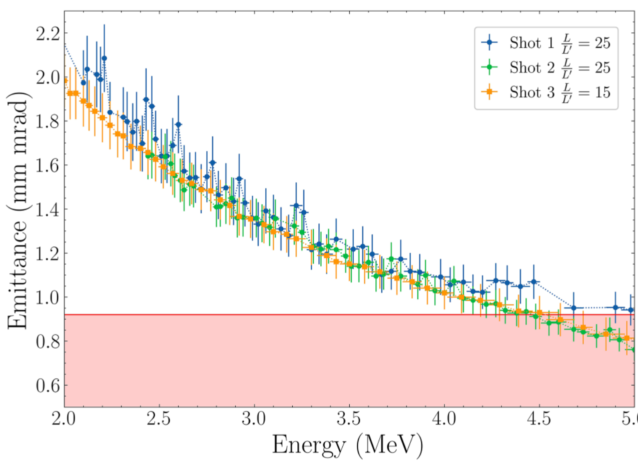

FIG. 4. Geometrical emittance at different proton energies for three nonconsecutive shots with trace magnification $L'/L = 25$ (circles) and $L'/L = 15$ (squares). Red shaded area shows the calculated device resolution limit.

method can be found at convoluted trace divergences smaller that the PSF, yielding a detection threshold of $\varepsilon_{\rm rms,min} = 0.92$ mm mrad. This limit can be easily overcome by means of smaller pinholes.

In addition, proton scattering in the bulk of the plastic scintillator was considered in the estimation of the trace thicknesses. Following the corrected Highland's formula for multiple scattering [33,34] integrated along the scintillator depth, the apparent trace widening was calculated for different proton energies, and the corresponding correction was applied to the measurement.

Figure 4 shows the energy-resolved emittance of the proton beam for three different shots with two different magnification configurations. Proton energies well above 10 MeV were detected, despite not being shown due to the diagnostic resolution limit. The shot-to-shot emittance variations averaged 3%.

For sake of comparison with previous results, the normalized emittance for each *energy slice* (i.e., considering monochromaticity) can be estimated following Eq. (3) for $\sigma_E = 0$, resulting in $\varepsilon_{n,\rm rms} \approx \beta\epsilon_{\rm rms}$. Figure 5 shows the normalized value for the average of the shots shown in Fig. 4. The results obtained in this study are consistent with previous research (see Fig. 1).

Due to the small shot-to-shot emittance variations shown in Fig. 4, and taking benefit of the HRR compatibility of the detector, traces measured in separated shots with different transverse detector locations could be merged into a single estimation of the emittance, spanning a larger horizontal angle than in a single shot. Figure 6 shows the emittances calculated after joining eight traces from eight evenly distributed pinhole horizontal positions measured in four different shots, spanning a total beam horizontal angle of 13.4°. This process was repeated at three different vertical angles. Since different transverse angles were measured in separated shots and merged in a single emittance value, it is important to note that the shot-to-shot laser pointing instability could led to an artificial enhancement of the estimated emittance through variations of the beamlet positions in the detector $\langle x_i' \rangle$

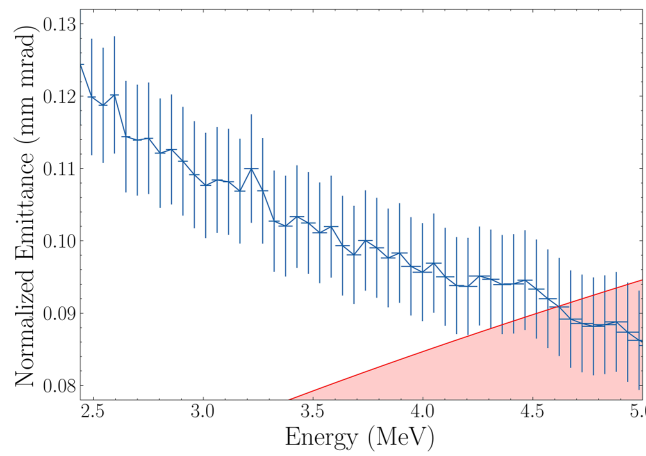

FIG. 5. Normalized emittance averaged from the shots shown in Fig. 4. Red shaded area shows the calculated device resolution limit.

between shots. This effect was corrected by constraining the beamlet positions of the merged traces onto their geometrical projections according to the pinhole mask movement. The corresponding uncertainty due to this assumption was included in the total emittance error estimation, following a pointing stability evaluation.

IV. DISCUSSION

The *B*-field streaked pepper-pot is an HRR-compatible emittance diagnostic for broadband laser-driven proton beams. The most commonly used previous methodologies (i.e., the grid radiography [12–15] and microfocusing fiducials [16–18]) showed notable trace-space emittance results but with several technical limitations, such as the lack of fine energy resolution (due to the use of RCF as a final detector) or low-repetition-rate compatibility. Moreover, in most of the cases, the results are estimated by the reconstruction of the particles' virtual source, which simply yields an upper limit to the emittance. Several alternatives for emittance estimation

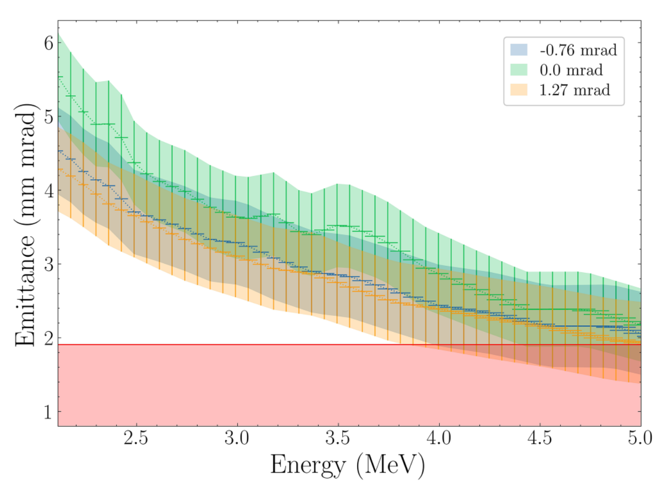

FIG. 6. Geometrical emittance at three different vertical beam coordinates. Each emittance value was calculated by mergeing data obtained in four separated shots.

for laser-driven proton beams can be found in Ref. [19], but in any case for a narrowband selection of the complete spectrum. It is worth mentioning the work of Ref. [29], where a modification of the pepper pot with a permanent magnet quadrupole triplet permitted the measurement of the transverse emittance of laser-driven electron beams with energy spread below 1%.

On the other hand, the methodology shown permits the beam phase-space retrieval of a broadband beam due to its extended spectral resolution. By simultaneous measurement of the beam energy spread σ_E and the geometrical emittance $\varepsilon_{\mathrm{rms}}$, the streaked pepper pot could estimate the phase-space normalized emittance for broad-spectrum beams through Eq. (3), mandatory for calculating the emittance growth of laser-driven proton beams and useful for the optimized design of corresponding beamlines [20,22]. This will be the scope of a future work, since it requires the absolute calibration of the response curve of the plastic scintillators.

It is important to mention that, despite being normally ignored in the pepper-pot technique, the noninfinitely small size of the pinholes should be considered, both in the transverse coordinate X (as already discussed above by PSF deconvolution) and in the magnetic deflection direction. In the latter case, it results in a spectral *mixing* of the detected traces. However, this effect will be enormously suppressed by means of smaller pinholes in a future work. Conversely, both the pinhole vignetting effect and the difference between the lowest and highest energy particles in flight path were estimated to be minor and hence ignored in the analysis.

V. CONCLUSION AND PERSPECTIVES

In this work, a different diagnostic for the trace space of laser-driven proton beams is presented. Its excellent spectral resolution paves the way for understanding the correlation between beam transverse dynamics and energy in these broadband beams, enabling a more accurate assessment of the normalized emittance. Furthermore, its compatibility with HRR meets the requirements of the next generation of tabletop laser accelerators.

A future work will address the limitations found in a more refined version of the detector: increased angular acceptance toward a complete beam single-shot retrieval, spectral and spatial resolution improvement (by means of smaller pinholes), and detector charge absolute calibration. Moreover, after a dedicated design and by means of wedged electrical plates and dipole, separated ion species detection could be achieved with simultaneous electric field deflection, following the operation principle of a TP spectrometer, as proposed in Ref. [35].

The standardization of the streaked pepper pot could be applied not only for its implementation in HRR beamlines [11,19], but also in the investigation of TNSA in specially shaped target, as in the case of the hemispherical target in the scheme for proton fast ignition [6,7], as well as in laser-driven ion acceleration mechanism research [36–40]. This technique could also be extended in laser-driven electron accelerators. The present work, despite covering proton energies up to a few MeV, can be of interest for several current applications, such as the beam evaluation in particle stopping power measurements in plasmas [41].

ACKNOWLEDGMENTS

The authors acknowledge support from Project No. PID2022-137339OB-C21, funded by MICIU/AEI/10.13039/501100011033/FEDER, UE, Project No. CLP263P20, funded by Goverment of Castilla y León, co-financed with FEDER funds, and Grant No. PID2021-125389OA-I00, funded by MICIU/AEI/10.13039/501100011033/FEDER, UE and "ERDF, a way of making Europe," UE. The authors would also like to thank S. Núñez for the fruitful discussions, as well as to the CLPU team for their excellent support.

DATA AVAILABILITY

The data that support the findings of this article are openly available [42].

[1] A. Macchi, M. Borghesi, and M. Passoni, Ion acceleration by superintense laser-plasma interaction, Rev. Mod. Phys. **85**, 751 (2013).

[2] H. Daido, M. Nishiuchi, and A. S. Pirozhkov, Review of laser-driven ion sources and their applications, Rep. Prog. Phys. **75**, 056401 (2012).

[3] B. Dromey, M. Coughlan, L. Senje, M. Taylor, S. Kuschel, B. Villagomez-Bernabe, R. Stefanuik, G. Nersisyan, L. Stella, J. Kohanoff, M. Borghesi, F. Currell, D. Riley, D. Jung, C.-G. Wahlström, C. Lewis, and M. Zepf, Picosecond metrology of laser-driven proton bursts, Nat. Commun. **7**, 10642 (2016).

[4] M. Borghesi, A. Schiavi, D. H. Campbell, M. G. Haines, O. Willi, A. J. Mackinnon, P. Patel, M. Galimberti, and L. A. Gizzi, Proton imaging detection of transient electromagnetic fields in laser-plasma interactions (invited), Rev. Sci. Instrum. **74**, 1688 (2003).

[5] J. J. Santos, M. Bailly-Grandvaux, L. Giuffrida, P. Forestier-Colleoni, S. Fujioka, Z. Zhang, P. Korneev, R. Bouillaud, S. Dorard, D. Batani, M. Chevrot, J. E. Cross, R. Crowston, J.-L. Dubois, J. Gazave, G. Gregori, E. d'Humières, S. Hulin, K. Ishihara, and S. Kojima, Laser-driven platform for generation and characterization of strong quasi-static magnetic fields, New J. Phys. **17**, 083051 (2015).

[6] P. K. Patel, A. J. Mackinnon, M. H. Key, T. E. Cowan, M. E. Foord, M. Allen, D. F. Price, H. Ruhl, P. T. Springer, and R. Stephens, Isochoric heating of solid-density matter with an ultrafast proton beam, Phys. Rev. Lett. **91**, 125004 (2003).

[7] M. Roth, T. E. Cowan, M. H. Key, S. P. Hatchett, C. Brown, W. Fountain, J. Johnson, D. M. Pennington, R. A. Snavely, S. C. Wilks, K. Yasuike, H. Ruhl, F. Pegoraro, S. V. Bulanov, E. M. Campbell, M. D. Perry, and H. Powell, Fast ignition by intense laser-accelerated proton beams, Phys. Rev. Lett. **86**, 436 (2001).

[8] K. Batani, Perspectives on research on laser driven proton-boron fusion and applications, J. Instrum. **18**, C09012 (2023).

[9] M. R. D. Rodrigues, A. Bonasera, M. Scisciò, J. A. Pérez-Hernández, M. Ehret, F. Filippi, P. L. Andreoli, M. Huault,

H. Larreur, D. Singappuli, D. Molloy, D. Raffestin, M. Alonzo, G. G. Rapisarda, D. Lattuada, G. L. Guardo, C. Verona, F. Consoli, G. Petringa, and A. McNamee, Radioisotope production using lasers: From basic science to applications, Matter Radiat. Extremes **9**, 037203 (2024).

[10] F. Kroll *et al.*, Tumour irradiation in mice with a laser-accelerated proton beam, Nat. Phys. **18**, 316 (2022).

[11] T. Cebriano Ramírez, A. Curcio, J. I. Apiñaniz, D. De Luis, A. Morabito, C. Salgado-López, E. Filippov, M. D. Rodríguez Frías, L. Volpe, and G. Gatti, Design and implementation of the first proton beam transport line in vega-3 petawatt laser system, Sci. Rep. **14**, 29935 (2024).

[12] M. Borghesi, A. J. Mackinnon, D. H. Campbell, D. G. Hicks, S. Kar, P. K. Patel, D. Price, L. Romagnani, A. Schiavi, and O. Willi, Multi-MeV proton source investigations in ultraintense laser-foil interactions, Phys. Rev. Lett. **92**, 055003 (2004).

[13] P. T. Campbell, D. Canning, A. E. Hussein, K. D. W. Ratnayaka, A. G. R. Thomas, K. Krushelnick, and L. Willingale, Proton beam emittance growth in multipicosecond laser-solid interactions, New J. Phys. **21**, 103021 (2019).

[14] S. Ter-Avetisyan, P. K. Singh, M. H. Cho, A. Andreev, K. F. Kakolee, H. Ahmed, C. Scullion, S. Sharif, P. Hadjisolomou, and M. Borghesi, Proton acceleration through a charged cavity created by ultraintense laser pulse, Phys. Plasmas **26**, 103106 (2019).

[15] P. K. Singh, P. Varmazyar, B. Nagy, J.-G. Son, S. Ter-Avestiyan, and K. Osvay, Low divergent MeV-class proton beam with micrometer source size driven by a few-cycle laser pulse, Sci. Rep. **12**, 8100 (2022).

[16] T. E. Cowan *et al.*, Ultralow emittance, multi-MeV proton beams from a laser virtual-cathode plasma accelerator, Phys. Rev. Lett. **92**, 204801 (2004).

[17] M. Roth, E. Brambrink, P. Audebert, A. Blazevic, R. Clarke, J. Cobble, T. E. Cowan, J. Fernandez, J. Fuchs, M. Geissel *et al.*, Laser accelerated ions and electron transport in ultra-intense laser matter interaction, Laser Part. Beams **23**, 95 (2005).

[18] F. Nürnberg, M. Schollmeier, E. Brambrink, A. Blažević, D. C. Carroll, K. Flippo, D. C. Gautier, M. Geißel, K. Harres, B. M. Hegelich, O. Lundh, K. Markey, P. McKenna, D. Neely, J. Schreiber, and M. Roth, Radiochromic film imaging spectroscopy of laser-accelerated proton beams, Rev. Sci. Instrum. **80**, 033301 (2009).

[19] M. J. Wu, D. Y. Li, J. G. Zhu, T. Yang, X. Y. Hu, Y. X. Geng, K. Zhu, M. J. Easton, Y. Y. Zhao, A. L. Zhang, H. Y. Lu, W. J. Ma, C. Lin, and X. Q. Yan, Emittance measurement along transport beam line for laser driven protons, Phys. Rev. Accel. Beams **23**, 031302 (2020).

[20] M. J. Wu, D. Y. Li, T. Yang, Y. Z. Li, H. Cheng, Y. D. Xia, Y. Yan, Y. L. Fang, K. Zhu, M. J. Easton, C. Lin, and X. Q. Yan, Emittance growth analysis of laser-driven broad energy spectral proton beams, Phys. Rev. Accel. Beams **27**, 041303 (2024).

[21] A. J. Kemp, J. Fuchs, Y. Sentoku, V. Sotnikov, M. Bakeman, P. Antici, and T. E. Cowan, Emittance growth mechanisms for laser-accelerated proton beams, Phys. Rev. E **75**, 056401 (2007).

[22] K. Floettmann, Some basic features of the beam emittance, Phys. Rev. Spec. Top. Accel. Beams **6**, 034202 (2003).

[23] S. Humphries, *Charged Particle Beams* (Dover, Mineola, NY, 2013).

[24] M. Migliorati, A. Bacci, C. Benedetti, E. Chiadroni, M. Ferrario, A. Mostacci, L. Palumbo, A. R. Rossi, L. Serafini, and P. Antici, Intrinsic normalized emittance growth in laser-driven electron accelerators, Phys. Rev. Spec. Top. Accel. Beams **16**, 011302 (2013).

[25] M. Zhang, Emittance formula for slits and pepper-pot measurement, Technical report, Fermi National Accelerator Laboratory (1996), https://lss.fnal.gov/archive/test-tm/1000/fermilab-tm-1988.pdf.

[26] S. Fritzler, E. Lefebvre, V. Malka, F. Burgy, A. E. Dangor, K. Krushelnick, S. P. D. Mangles, Z. Najmudin, J.-P. Rousseau, and B. Walton, Emittance measurements of a laser-wakefield-accelerated electron beam, Phys. Rev. Lett. **92**, 165006 (2004).

[27] C. M. S. Sears, A. Buck, K. Schmid, J. Mikhailova, F. Krausz, and L. Veisz, Emittance and divergence of laser wakefield accelerated electrons, Phys. Rev. Spec. Top. Accel. Beams **13**, 092803 (2010).

[28] E. Brunetti, R. P. Shanks, G. G. Manahan, M. R. Islam, B. Ersfeld, M. P. Anania, S. Cipiccia, R. C. Issac, G. Raj, G. Vieux, G. H. Welsh, S. M. Wiggins, and D. A. Jaroszynski, Low emittance, high brilliance relativistic electron beams from a laser-plasma accelerator, Phys. Rev. Lett. **105**, 215007 (2010).

[29] G. G. Manahan, E. Brunetti, C. Aniculaesei, M. P. Anania, S. Cipiccia, M. R. Islam, D. W. Grant, A. Subiel, R. P. Shanks, R. C. Issac, G. H. Welsh, S. M. Wiggins, and D. A. Jaroszynski, Characterization of laser-driven single and double electron bunches with a permanent magnet quadrupole triplet and pepper-pot mask, New J. Phys. **16**, 103006 (2014).

[30] C. Salgado-López, J. I. Apinaniz, J. L. Henares, J. A. Pérez-Hernández, D. de Luis, L. Volpe, and G. Gatti, Angular-resolved Thomson parabola spectrometer for laser-driven ion accelerators, Sensors **22**, 3239 (2022).

[31] R. Nedbailo, J. Park, R. Hollinger, S. Wang, D. Mariscal, J. Morrison, H. Song, G. Zeraouli, G. G. Scott, T. Ma, and J. J. Rocca, Compact high repetition rate Thomson parabola ion spectrometer, Rev. Sci. Instrum. **94**, 023505 (2023).

[32] J. A. Kulesza *et al.*, MCNP® Code version 6.3.0 theory & user manual, Technical report LA-UR-22-30006, Rev. 1, Los Alamos National Laboratory, Los Alamos, NM, USA (2022).

[33] V. L. Highland, Some practical remarks on multiple scattering, Nucl. Instrum. Methods **129**, 497 (1975).

[34] G. R. Lynch and O. I. Dahl, Approximations to multiple Coulomb scattering, Nucl. Instrum. Methods Phys. Res. Sect. B **58**, 6 (1991).

[35] S. Kojima, S. Inoue, T. H. Dinh, N. Hasegawa, M. Mori, H. Sakaki, Y. Yamamoto, T. Sasaki, K. Shiokawa, K. Kondo, T. Yamanaka, M. Hashida, S. Sakabe, M. Nishikino, and K. Kondo, Compact Thomson parabola spectrometer with variability of energy range and measurability of angular distribution for low-energy laser-driven accelerated ions, Rev. Sci. Instrum. **91**, 053305 (2020).

[36] S. Kar, K. F. Kakolee, B. Qiao, A. Macchi, M. Cerchez, D. Doria, M. Geissler, P. McKenna, D. Neely, J. Osterholz, R. Prasad, K. Quinn, B. Ramakrishna, G. Sarri, O. Willi, X. Y. Yuan, M. Zepf, and M. Borghesi, Ion acceleration in multi-species targets driven by intense laser radiation pressure, Phys. Rev. Lett. **109**, 185006 (2012).

[37] D. Haberberger, S. Tochitsky, F. Fiuza, C. Gong, R. A. Fonseca, L. O. Silva, W. B. Mori, and C. Joshi, Collisionless shocks

in laser-produced plasma generate monoenergetic high-energy proton beams, Nat. Phys. **8**, 95 (2012).

[38] J. Henares, P. Puyuelo-Valdes, C. Salgado-López, J. Apiñaniz, P. Bradford, F. Consoli, D. de Luis, M. Ehret, F. Hannachi, R. Hernández-Martín *et al.*, Proton and helium ions acceleration in near-critical density gas targets by short-pulse Ti:Sa PW-class laser, J. Plasma Phys. **89**, 965890601 (2023).

[39] V. Ospina-Bohórquez, C. Salgado-López, M. Ehret, S. Malko, M. Salvadori, T. Pisarczyk, T. Chodukowski, Z. Rusiniak, M. Krupka, P. Guillon, M. Lendrin, G. Pérez-Callejo, C. Vlachos, F. Hannachi, M. Tarisien, F. Consoli, C. Verona, G. Prestopino, J. Dostal, and R. Dudzak, Laser-driven ion and electron acceleration from near-critical density gas targets: Towards high-repetition rate operation in the 1 PW, sub-100 fs laser interaction regime, Phys. Rev. Res. **6**, 023268 (2024).

[40] M. J. V. Streeter *et al.*, Stable laser-acceleration of high-flux proton beams with plasma collimation, Nat. Commun. **16**, 1004 (2025).

[41] S. Malko *et al.*, Proton stopping measurements at low velocity in warm dense carbon, Nat. Commun. **13**, 2893 (2022).

[42] C. Salgado-López, I. Rodríguez-Pérez, and J. I. Apiñaniz, Dataset spectral study of the lateral trace-space of laser-driven proton beams [Data set], Zenodo (2025), https://doi.org/10.5281/zenodo.15394680.